analytical chemistry

pubs.acs.org/ac

Article

Confinement of Monolithic Stationary Phases in Targeted Regions of 3D-Printed Titanium Devices Using Thermal Polymerization

Marta Passamonti,* Ischa L. Bremer, Suhas H. Nawada, Sinéad A. Currivan, Andrea F. G. Gargano, and Peter J. Schoenmakers

Cite This: *Anal. Chem.* 2020, 92, 2589−2596

Read Online

ACCESS | Metrics & More | Article Recommendations | Supporting Information

ABSTRACT: In this study, we have prepared thermally initiated polymeric monolithic stationary phases within discrete regions of 3D-printed titanium devices. The devices were created with controllable hot and cold regions. The monolithic stationary phases were first locally created in capillaries inserted into the channels of the titanium devices. The homogeneity of the monolith structure and the interface length were studied by scanning a capacitively coupled conductivity contactless detector (C^4D) along the length of the capillary. Homogeneous monolithic structures could be obtained within a titanium device equipped with a hot and cold jacket connected to two water baths. The confinement method was optimized in capillaries. The sharpest interfaces (between monolith and empty channel) were obtained with the hot region maintained at 70 °C and the cold region at 4 or 10 °C, with the latter temperature yielding better repeatability. The optimized conditions were used to create monoliths bound directly to the walls of the titanium channels. The fabricated monoliths were successfully used to separate a mixture of four intact proteins using reversed-phase liquid chromatography. Further chromatographic characterization showed a permeability (K_f) of ~4 × 10^{-15} m^2 and a total porosity of 60%.

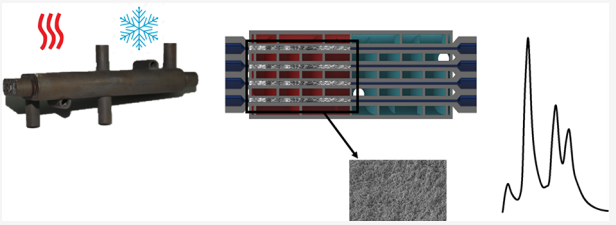

Since their introduction in the chromatographic world, porous polymer monoliths have proven to be powerful separation media. These chromatographic supports have been widely applied for applications, such as microscale liquid chromatography (LC) of peptides and proteins, but have also been used in capillary electrochromatography (CEC),[1] gas chromatography (GC),[2] sample preparation,[3] and catalysis.[4] The ease of preparation of monoliths, diverse chemistry options, and high permeabilities have made them popular materials for analytical devices, such as microfluidic chips for LC.

In the past decade, miniaturization has been realized by developing lab-on-a-chip solutions, where several analytical processes can be integrated within a few square centimeters. In such systems, due to the small channels and articulated geometries, the particle-packing procedure has proven to be challenging.[5] In contrast, monolithic beds are usually created *in situ* by free-radical polymerization of monomers in the presence of porogens and they are well-suited for chip-based separations. The proliferation of microfluidic devices has spurred new interest in polymer monoliths for applications such as enzymatic reactors[6,7] and microfluidic mixers.[8] This development has been boosted by the advent of additive manufacturing (or 3D-printing), which allows for rapid prototyping of complex structures, converting computer-aided-design (CAD) models into physical objects. Unfortunately, the use of 3D-printed analytical devices for chromatographic analysis is limited by the solvent compatibility of some materials (e.g., acrylate-based polymers) and in some cases by their transparency at the desired wavelength (e.g., UV or IR wavelengths). Several successful steps have been taken to locally photopolymerize monolithic stationary phases in discrete regions of microfluidic devices.[9−12]

Heat is an alternative way to transfer energy to the monomer precursors for initiating the polymerization. However, accurate control of temperature in small confined spaces is more difficult to achieve, and so far only few steps have been taken in this direction.[13]

In this work, two methods are explored to achieve confined thermal polymerization. The first approach involves direct contact (DC) between Peltier elements and the surface of a titanium device. In the second approach, recirculating jackets are used for localized heating and cooling (heating/cooling jackets, HCJ). The latter approach resembles a recirculation-based freeze−thaw valve.[14] In both approaches, defined hot (HR) and cold (CR) regions are created. We aim to fabricate poly(styrene-*co*-divinylbenzene) (PS-DVB) monolithic stationary phases within a 3D-printed titanium microfluidic

Received: September 20, 2019
Accepted: December 26, 2019
Published: December 26, 2019

https://dx.doi.org/10.1021/acs.analchem.9b04298
Anal. Chem. 2020, 92, 2589−2596

device through polymerization at 70 °C, and to separate intact proteins using this device.

EXPERIMENTAL SECTION

Materials. Styrene (STY, >99.5%), divinylbenzene (DVB, 80%), 3-(trimethoxysilyl)propyl methacrylate (γ-MAPS, 98%), 2,2′-azobis(isobutyronitrile) (AIBN, 98%), *n*-decanol (99%), sodium hydroxide (NaOH), aluminum oxide, lysozyme from chicken egg white (Lys), carbonic anhydrase from bovine heart (CA, >90%), cytochrome c from equine heart (CC, >95%), bovine casein (Cas), and potassium iodide (KI, >99%) were purchased from Sigma-Aldrich (St. Louis, Missouri, United States). Ethanol (EtOH), methanol (MeOH), acetonitrile (ACN), and tetrahydrofuran (THF, >99.8) were purchased from Biosolve (Valkenswaard, The Netherlands). Hydrochloric acid 37% (HCl) and glacial acetic acid were obtained from Acros (Geel, Belgium). Milli-Q water (18.2 MΩcm) was produced by a Sartorius Arium 611UV Ultrapure Water System (Göttingen, Germany). The titanium devices were purchased from Materialise (Leuven, Belgium), while the capillary (0.53 mm ID, 0.70 mm OD) was purchased from CMScientific (Silsden, UK).

Device Design and 3D-Printing. The direct contact (DC) device, shown in Figure 1a, contains two 40 × 40 mm^2 pads for two Peltier elements to be attached on the hot (red) and cold (blue) sides. A wall thickness of 1 mm was designed between the channels (1 mm ID) and the Peltier element pads.

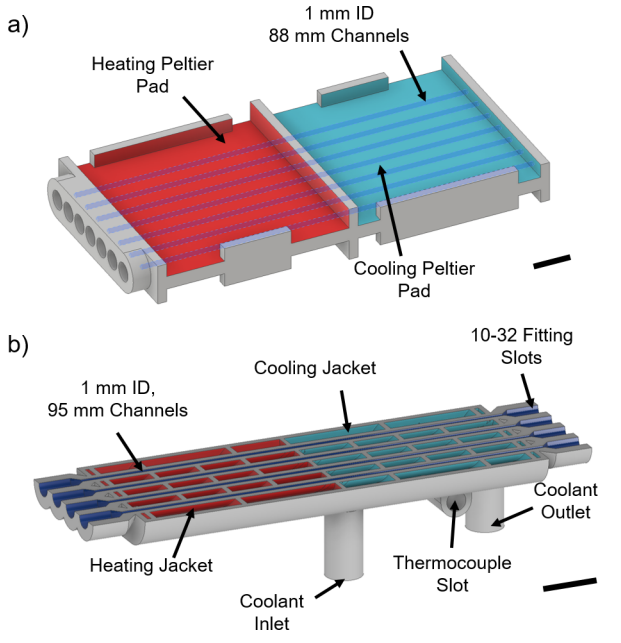

Figure 1. CAD images of the two devices: (a) Direct contact (DC) device with two Peltier element pads for heating and cooling, (b) cross-sectional cutaway of the heating/cooling jacket (HCJ) device with two recirculating zones, jacket and thermocouple fittings. The scale bars in (a) and (b) represent 10 mm.

Figure 1b shows the heating−cooling jacket (HCJ) device, which contains two recirculating jackets, enveloping a set of four channels (1 mm ID, 95 mm length, 1 mm wall thickness). The HCJ device essentially contains a set of shell-and-tube heat exchangers maintaining temperatures of T_H (higher temperatures) and T_C (lower temperatures) in the two zones. For each jacket, inlet and outlet slots for the recirculating fluids were included, with a thermocouple slot to monitor the jacket temperature. To facilitate homogeneous recirculation across the jackets and to ensure a self-supporting geometry for 3D-printing, the jackets contained a series of baffle fins.

CAD files (Figure S5a,b) of the two models were designed using Autodesk Inventor 2018 (San Rafael, CA, USA). The model was 3D-printed with a selective-laser-melting (SLM) system (EOS M280 (EOS, Maisach, Germany)), using a Ti 6-4 alloy (90% titanium, 6% aluminum, 4% vanadium). 10-32 HPLC threads were then tapped into the fitting slots of the two pieces.

Experimental Setups. The DC device is in direct contact with four Peltier elements (TEC1-12706 Hebei, Shanghai, China): two attached to the HR, and two attached to the CR. Two CPU fans are placed on top of the latter as heat-sinks. Two temperature controllers (STC 1000, Inkbird, Shenzhen, China) for the CR and the HR were set at T_C = 19 °C and T_H = 70 °C, respectively, and monitored by two thermocouples, attached to the DC device.

The HCJ titanium device (Figure 1b) contains one inlet and one outlet for each jacket. The heating jacket is connected to a water bath (900F, Julabo, Seelbach, Germany) maintained at 72 °C. The thermocouple on the titanium device reported a temperature of 70 °C. The difference can be explained by heat dissipation through tubing connections. Continuous flow was pumped from the water bath to the titanium device (ca. 12 L/min).

An analogous method was used for controlling the cold region (CR) temperature (T_C). Different values of T_C were evaluated, while T_H was kept at 70 °C. The water bath (TC-602, Brookfield AM, Toronto, Canada) connected to the cooling jackets was set at 2, 8.6, 25, or 35 °C. The temperatures reported by the probe placed on the CR slot were 4, 10, 24, and 33 °C, respectively.

In Situ Synthesis of Monolithic Stationary Phases. After printing, the HCJ titanium device was heated at 5 °C/min up to 500 °C and kept at this temperature for 6 h in a furnace (AAF 1100, Carbolite Gero, Neuhausen, Germany). The device was then brought back to room temperature with a ramp of 10 °C/min. After etching the internal surface of the capillaries and the HCJ titanium device, they were rinsed for 10 min with water and dried with nitrogen as described by Courtois et al.[15]

The surfaces of the capillaries and the oxidized HCJ titanium device were silanized using a 20% (v/v) γ-MAPS solution prepared in EtOH with an approximate pH of 5, adjusted using glacial acetic acid. The solution was flushed through for 90 min at 10 μL/min. Thereafter, the surface-modified channels were flushed with EtOH and dried with nitrogen.

PS-DVB monolith was polymerized *in situ* within the capillaries, placed inside the HCJ titanium device. The monomer and the cross-linker were purified before use, using an alumina (Al_2O_3) bed. A polymerization mixture consisting of 20 wt % STY, 20 wt % DVB, 52 wt % 1-decanol, and 8 wt % THF was prepared, and each housing was filled. Thermal free-radical polymerization was initiated using 2 wt % AIBN with respect to the monomers, similarly to what was described by Vonk et al.[1] The polymerization mixture was sonicated for 15 min to ensure homogeneity, followed by 10 min purging with nitrogen to remove oxygen. The capillaries were filled by capillary force, sealed with rubber septa, and placed in the channels of the titanium devices. To uniformly fill the channels

https://dx.doi.org/10.1021/acs.analchem.9b04298
Anal. Chem. 2020, 92, 2589−2596

in the HCJ titanium device, the four outlets on the heating side (Figure 1b, left-hand side) were connected to capillaries, while the polymerization mixture was pushed through the channel with a syringe from the cold (right-hand) side. The capillaries were then sealed and the polymerization was performed at T_H = 70 °C for 24 h. After polymerization, the monolithic columns were thoroughly flushed with MeOH (>50 column volumes).

Physical Characterization of Polymer Monoliths. *Capacitively Coupled Contactless Conductivity Detection.* To investigate the nature of the interface between the polymerized and the empty zones, experiments were performed with polyimide-coated glass capillaries inserted into the DC and HCJ devices. This choice was mainly made to optimize the parameters of the polymerization (e.g., CR temperature), before synthesizing the monoliths directly in the devices. In the capillaries, we assessed the homogeneity of the stationary phase, the sharpness of the interface, and the repeatability using a capacitively coupled contactless conductivity detector (C^4D, TraceDec, Innovative Sensor Technologies, Innsbruck, Austria). The latter is a noninvasive on-capillary detection method. The C^4D was equipped with a probe, through which the monolithic capillary column was placed. By moving the detector along the length of the capillary, with a reference for length, a profile can be obtained.[16] The method is based on two ring electrodes which surround the capillary. It has been used successfully to characterize capillary coatings,[17] monoliths,[18] monolithic porous-layer open-tubular (PLOT) columns,[19] particle packed columns,[20] and graphene fibers.[21] The C^4D was used to assess the homogeneity of the monolith in the capillaries and to evaluate the sharpness of the interface, during setup optimization. Regions of homogeneous monolith or empty capillary are reflected in a stable response from the detector. While the capillary was flushed at 4 μL/min with MeOH, the conductivity was measured for each millimeter along the capillary, in triplicate. The C^4D parameters were kept constant for each capillary as follows: high frequency, 0 dB Volt, 50% gain, offset 0. The measured conductivity values (C_h) for each capillary were normalized to the highest value ($C_{h(max)}$, from the unmodified capillary segment), i.e., $C_h^* = C_h/C_{h(max)}$.

The attachment of the monolith to the capillary surface is another important feature that was investigated. In order to perform chromatographic separations, wall attachment is essential to avoid channeling or breakthrough. Permeability tests and scanning electron microscopy (SEM) images were used to evaluate the surface attachment.

Scanning Electron Microscopy. Scanning electron microscopy (SEM) experiments were performed on an FEI Verios 460 instrument (Thermo Fisher Scientific, Eindhoven, The Netherlands) equipped with an Everhart-Thornley detector (EDT) using a 2 kV electron beam. The samples were sputter-coated with a 20 nm gold layer.

Chromatographic Characterization. The performances of the monolithic columns were assessed in terms of chromatographic behavior, porosity, permeability, and repeatability. All chromatographic experiments were performed on a Waters Acquity UPLC system (Waters, Milford, MA, USA), which consisted of a binary solvent manager, a thermostated autosampler, an air-heated column compartment, and a dual-wavelength UV−vis (TUV) detector equipped with a 100 nL flow-cell.

Permeability and Porosity. The permeability (K_f) was evaluated using MeOH at 20 μL/min and 40 μL/min in all the capillaries and in the HCJ device using Darcy's law:[22]

$$K_f = \frac{F_m \eta L}{\Delta P \pi r^2} \quad (1)$$

where F_m is the flow rate of the solvent, η is the dynamic viscosity of the solvent, L is the length of the monolith, ΔP is the pressure drop across the monolithic column, and r is the radius of the column.

Since the SLM process used to 3D-print the titanium devices uses irregularly shaped metal particles with a particle size range of 100−300 μm, the diameter and circularity of the HCJ channels may not be exactly as designed. An unretained compound (KI, isocratic elution in water at 35 μL/min) was used to determine the void volume (V_0) of the channel. The same channel was characterized in three different states, viz., empty (EC), fully polymerized (FC), and half polymerized (HC). FC and HC were fabricated by introducing the precursors into the channel and polymerizing with T_H at 70 °C and T_C at 70 and 10 °C, respectively. Each injection was repeated three times. The residence volume outside the channel was determined by three injections of KI without the HCJ device installed, and this was subtracted from all measured V_0 values.

Visual inspection and C^4D could not be used to study the confinement of the thermal polymerization in the HCJ. Instead, we used eq 2 to determine the percentage of monolithic stationary phase formed.

$$\mathrm{HC\%} = \left[1 - \left(\frac{t_{0(\mathrm{HC})} - t_{0(\mathrm{FC})}}{t_{0(\mathrm{EC})} - t_{0(\mathrm{FC})}}\right)\right] \times 100 \quad (2)$$

The t_0 values were used to calculate the total porosity (ε_T) according to eq 3[23]

$$\varepsilon_T = \frac{V_0}{V_g} = \frac{t_0 \times F_m}{V_g} \quad (3)$$

where V_g is the geometric volume of the channel, F_m is the flow rate of the solvent, and t_0 is the channel dead time.

In three channels, the PS-DVB monolithic stationary phase was created with T_C = 10 °C, and these channels were tested for the separations of proteins. A gradient (with Milli-Q water as mobile phase A and ACN as mobile phase B, both containing 0.1% (v/v) TFA; F_m = 35 μL/min) was employed at room temperature, using a 1 μL full-loop injection. The chromatographic performance was assessed using a test mixture of four proteins, i.e., lysozyme, carbonic anhydrase, cytochrome c, and bovine casein.

RESULTS AND DISCUSSION

Comparison of DC and HCJ Devices Using Inserted Capillaries. PS-DVB monoliths were created by thermal polymerization inside capillaries, which were inserted in either the DC or the HCJ device. The C^4D scanning profiles show the detector signal across the length of the capillary. In Figure 2, lower conductivities correspond to higher densities of monolithic material (created in the HR of the capillary), while higher conductivities correspond to empty (unpolymerized) parts of the capillary (CR). A constant conductivity response across the capillary reveals a homogeneous structure of the monolithic stationary phase.[20] An ideal result from our

https://dx.doi.org/10.1021/acs.analchem.9b04298
Anal. Chem. 2020, 92, 2589−2596

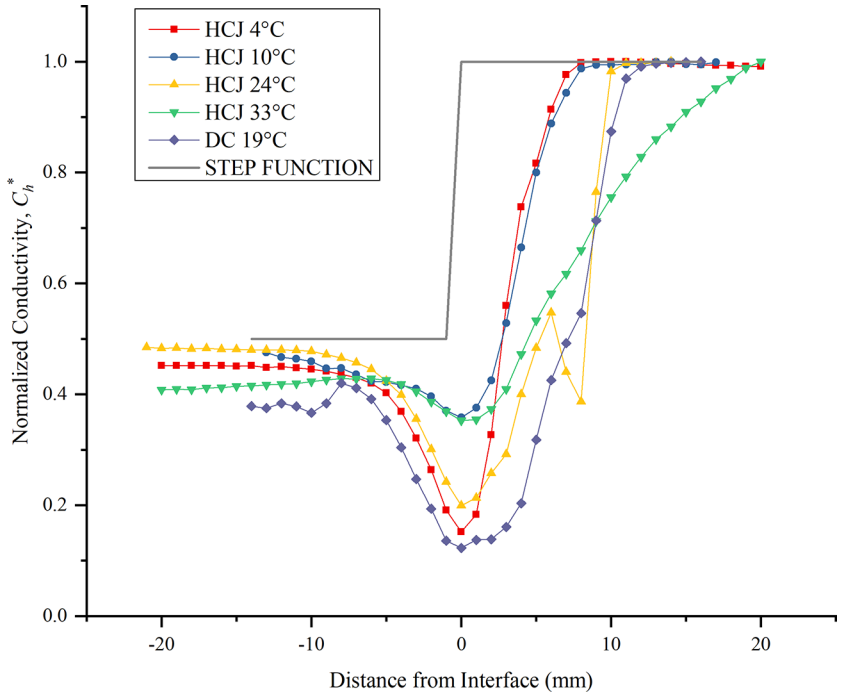

Figure 2. C^4D scanning profiles of four different capillary columns made within the HCJ device, respectively, with the CR at 4 °C (red, square), 10 °C (blue, circle), 24 °C (yellow, triangle), and 33 °C (green, inverted triangle), DC device 19 °C (purple, diamonds); and in gray the ideal step function is shown. The lower conductivity is characteristic for the monolithic stationary phase, while the empty capillary gives the higher conductivity.

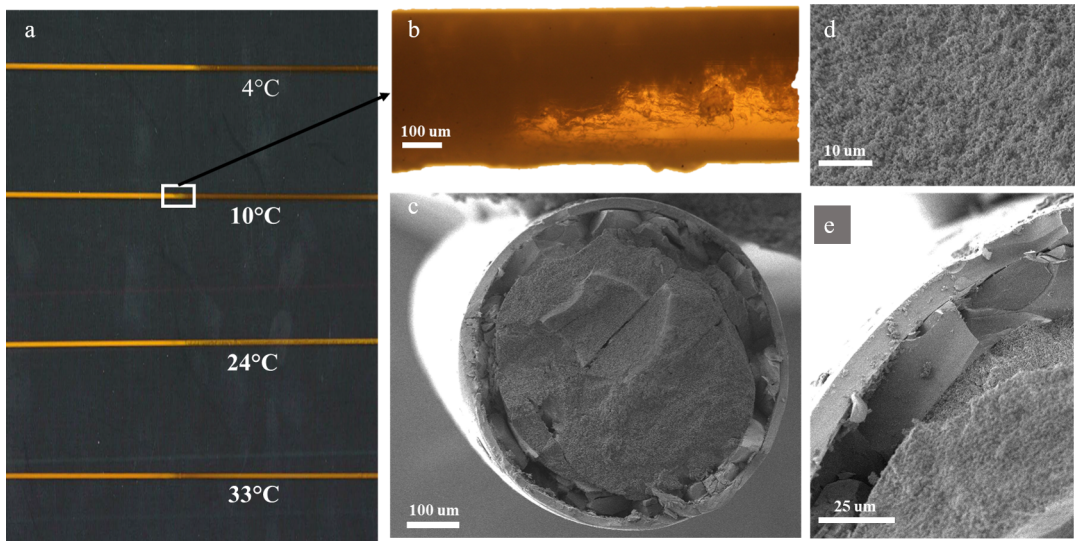

Figure 3. Images of PS-DVB monoliths created in capillaries placed into the HCJ device. (a) Top to bottom: 4 capillary columns made at T_C = 4, 10, 24, and 33 °C, respectively; (b) image of the interface between the CR (empty) and HR (polymerized); (c) SEM micrograph of a section of the main body of a capillary; (d) SEM micrograph of a monolithic stationary phase showing a homogeneous microglobular structure; (e) wall attachment area for a monolith inside a capillary.

confined-polymerization experiments would be a C^4D profile that shows a step function with constant conductivity signals on either side of the capillary housing (HR and CR). A sharp or nearly vertical interface between the two zones demonstrates successful confinement.[16] This ideal profile is schematically indicated by a gray line in Figure 2 (the absolute conductivities at the high and low end of this curve are not relevant).

Figure 2 shows a number of C^4D profiles obtained. In all profiles, a significant dip in the C^4D signal is evident at the end of the CR, causing the experimental curves to deviate from a stepwise or sigmoidal profile. The decrease in conductivity indicates an increase in the density of the polymeric structure. When the monolith is being formed in the HR, the monomer concentration is reduced, while in the CR, the monomer concentration remains constant. A potential reason may be that the free monomers and inactive initiator diffuse from the CR to the HR, in accordance with Fick's law of diffusion.[16] Thus, more STY and DVB monomer will be within reach of the free radicals, leading to the formation of a high-density frit-

https://dx.doi.org/10.1021/acs.analchem.9b04298
Anal. Chem. 2020, 92, 2589−2596

like structure. Another possible explanation can be thermal convection within the channel, as hinted at by the asymmetric gradient in Figure 3b. As a result, the polymerization section of the capillary was consistently about 55 mm long, as opposed to the designed 47.5 mm. In standard fabrication of polymer monolithic columns, the ends of the capillary are typically removed to overcome interface phenomena. However, this is not possible within 3D-printed channels.

When using the DC device, which relies on four Peltier elements directly attached to the printed piece, the hot and cold temperatures were set to 70 and 19 °C, respectively. The one DC curve shown in Figure 2 (purple diamonds and connecting line) shows a somewhat diffuse transition from the monolith region (HR, left-hand side) to the empty region (HC, right-hand side), extending over more than 10 mm of capillary length. Perhaps even more importantly, the monolith does not seem to be homogeneous as can be seen from the variations in the signal. Several HCJ curves are shown, obtained with different CR temperatures. The constant signals in the HR region indicate that homogeneous monoliths have been obtained. Generally, sharper transitions are obtained at lower CR temperatures. At T_C = 33 °C, the transition is very gradual (green line and inverted triangle), but at T_C = 24 °C, the transition is already sharper than when using the DC device (with T_C = 19 °C). At even lower temperatures, the main ramp stretches over much less than 10 mm. The results indicate better temperature control in the HCJ device than in the DC device. During the polymerization, the temperature controllers on both zones of the DC device showed fluctuations in temperature of ±5 °C, which may explain inhomogeneities in the resulting monoliths. In contrast, the two jackets of the HCJ setup were connected to two water baths. The large reservoirs of water and the corresponding high thermal mass provided stable temperatures during the entire polymerization process (24 h). Little fluctuation was detected by the temperature controllers (<0.5 °C), resulting in more homogeneous monoliths. Further experimental work was continued only with the HCJ device.

Thermal Confinement in HCJ Device. In order to test the effects of T_C on the interface, the CR of the HCJ was set at four different temperatures, i.e., T_C = 4, 10, 24, and 33 °C. At T_C = 4 °C, freezing of *n*-decanol may be possible (melting point 6.4 °C). To evaluate the repeatability of confined monolithic stationary phases in capillaries, three batches for each temperature were produced. These capillaries were then assessed using microscopy and C^4D measurements. Figure 3 shows some examples of the images that were obtained.

Figure 3 shows that confinement was achieved using T_C = 4 and 10 °C, but not in the 24 and 33 °C (left-side frame). The rate of AIBN initiation is related to the temperature. At the higher T_C values, the polymerization mixture partially polymerized, even within the intended empty region. At T_C = 33 °C, a clear interface could not be observed. At T_C= 24 °C, an interface was discernible (see Figure 2), but the polymer monolith was also being formed in the CR, and so the interface length reached almost 18 mm (see Table 1). Better confinement was obtained at T_C = 4 °C and T_C = 10 °C.

A quantitative summary of the C^4D profiles obtained is presented in Table 1. The stable monolith conductivity (C_h*) was defined as the average of the first 11 cm of the HR and normalized for each capillary. The interface length (L_i) was evaluated as the distance between the point where a 5% drop in the stable monolith conductivity was observed to the point where 95% of the value corresponding to the empty capillary was reached. The depth of the dip ΔC_0 in conductivity was measured as the difference between C_h* and the normalized conductivity at the 0 mm point on the horizontal axis. The steepness, S_L, of the profile at the interface is defined as the maximum gradient in the sigmoidal profile (see Figure 2).

Table 1. Batch-to-Batch (3 Batches, 8 Capillaries in Total) and Intrabatch (n = 3) Variation of Interface Length (L_i), Conductivity (C_h*), Dip (ΔC_0), and Steepness (S_L) of Monolithic Stationary Phases Prepared in Capillaries Inserted in the HCJ Device at Different CR Temperatures (T_C)

T_C (°C)	L_i (mm)	C_h*	ΔC_0	S_L (1/mm)
		Interbatch		
4	15.6 ± 2.45	0.42 ± 0.04	0.20 ± 0.07	0.24 ± 0.05
10	13.8 ± 2.37	0.43 ± 0.02	0.27 ± 0.04	0.25 ± 0.05
24	17.9 ± 3.06	0.45 ± 0.03	0.24 ± 0.07	0.25 ± 0.07
33	x	0.55 ± 0.09	0.22 ± 0.10	0.13 ± 0.09
		Intrabatch		
4	13.7 ± 0.47	0.39 ± 0.04	0.18 ± 0.02	0.21 ± 0.02
10	12.7 ± 0.47	0.43 ± 0.00	0.27 ± 0.03	0.24 ± 0.05
24	18 ± 1.63	0.46 ± 0.02	0.23 ± 0.07	0.21 ± 0.02
33	x	0.55 ± 0.09	0.21 ± 0.10	0.08 ± 0.02

The smallest values for L_i are obtained at the lowest values for T_C. The difference in interface length between experiments performed at T_C = 4 °C and those at T_C = 10 °C is less than 2 mm. The monolith conductivity (C_h) does not vary much with T_C (except for T_C = 33 °C, where no interface is observed). The intrabatch and interbatch standard deviations are low for each value of T_C. As the device contains four different channels suitable for polymerization, the potential variation in monolith formation due to thermal inconsistencies (brought about by channel location, e.g., edge or center) was also evaluated (Table 1). The polymerization is found to be only slightly affected by the channel in which it is performed, as the intrabatch variations indicate. The standard deviations at T_C = 10 °C are much lower than those obtained at T_C = 4 °C. Therefore, we selected T_H = 70 °C and T_C = 10 °C as temperatures to evaluate the chromatographic performances of the monolithic stationary phases created in the HCJ.

To apply the HCJ confinement method to a complex microfluidic chip such as the device for three-dimensional separations described by Wouters et al.,[24] the following considerations have to be made. To allow the interface between empty and polymerized zones, the location of the heating jacket must be offset by 15 mm from the desired location of the monolith. As shown by the C^4D profiles and confirmed by the SEM micrographs, the interface presents a higher polymer density, which is likely to show a lower permeability than the main separation body. The 4% variability in the length of the interface within batches and the 17% between batches provides an indication of what may be expected in applying the HCJ approach to polymerization in multiple channels of a microfluidic chip.

The thermal confinement of polymerization does not rely on the precision of laser-assisted photopolymerization described by Thurumann et al.,[10] nor on a photomask as described by Yu et al.[25] Confinement of UV-initiated polymerization is technically easier than confinement of thermal polymerization, but it requires substrates that are transparent at the wavelength used for initiation. Our method represents a complementary

https://dx.doi.org/10.1021/acs.analchem.9b04298
Anal. Chem. 2020, 92, 2589−2596

solution that can be applied to a wide variety of materials and designs with good repeatability.

Monolith Characterization. As mentioned above, a PS-DVB monolith was bound to the wall of the titanium HCJ device. Such stationary phases were created in three channels, with T_H = 70 °C and T_C = 10 °C. Plots of the column backpressure as a function of MeOH at 20 and 40 μL/min were used to assess the permeability of monoliths created using both inserted capillaries, and those fabricated directly in the HCJ device. In the HCJ monolith, other chromatographic tests, such as those measuring the porosity and separating intact proteins, were also performed.

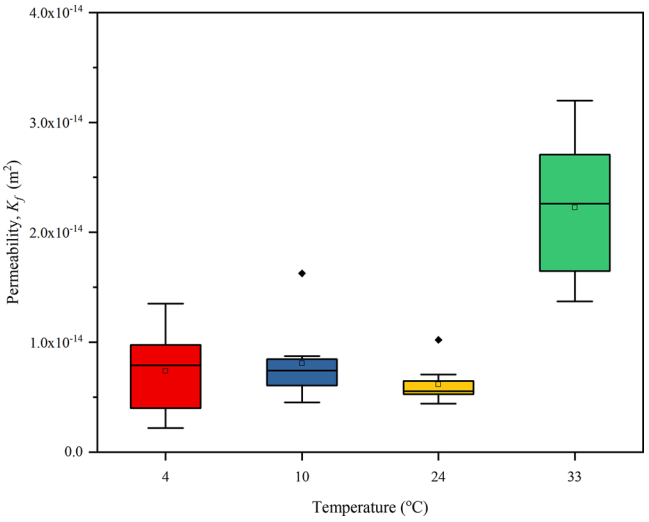

Figure 4. Interbatch permeability of the monolithic stationary phases created in capillaries for different values of the cold-region temperature (T_C). Eight columns were created and characterized for each T_C. Black dots are outliers.

In Figure 4, the ranges of observed permeability values (K_f; see eq 1) are indicated for each value of T_C. The K_f values obtained with T_C = 4 °C exhibit greater variability than those obtained with T_C = 10 °C (see Figure 4). Despite an outlier, the columns prepared with a T_C = 10 °C showed a more uniform permeability throughout the sample set. Using this information, monoliths were created directly in the HCJ device, with T_H = 70 °C and T_C = 10 °C. The permeability of the PS-DVB monoliths created directly in the HCJ (K_f = (4.04 ± 1.96) × 10^{-15} m^2, n = 3) was approximately half that of the capillary housed monolithic columns (K_f = (8.08 ± 0.65) × 10^{-15} m^2, n = 3), prepared with the same temperature settings. These values are in the same range as those reported by Vonk et al.[26] When several monoliths are created simultaneously in different channels within a single device, similar variations in the permeability may be observed as those shown in Figure 4 for T_C = 10 °C.

Potassium iodide (KI) was injected as an unretained marker in an empty-channel (EC) control, with the monolith synthesized directly within the HCJ device, polymerizing half of the channel (HC) or the full channel (FC). The t_0 values for EC, HC, and FC were 2.65, 2.35, and 2.08 min, respectively (see Figure S2). The former value was used to calculate the true diameter of the HCJ device. The t_0 peak indicates an ID of 0.91 mm, while the design value was 1 mm. The discrepancy is probably caused by inaccuracies in the SLM process. Using the true ID, we can infer that 53% of the channel was occupied by the PS-DVB stationary phase (cf., eq 2), whereas in capillaries this was 57%. A value closer to the targeted 50% suggests that direct synthesis on the HCJ walls results in better thermal confinement, possibly due to more efficient heat transfer from the jackets to the monomer mixture.

The t_0 values were used to calculate the total porosity, ε_T, for the HC and the FC, resulting in values of 60% and 67%, respectively. The difference is possibly due to the variation in polymer density at the interface. The injection of KI as an unretained marker can be used to confirm the repeatability of retention times and of the overall length of the monoliths in the three channels of the HCJ.

Figure 5 shows a chromatogram obtained using the HCJ device for the separation of intact proteins. The chromatographic performance was evaluated by gradient-elution separation of a mixture of four proteins (i.e., lysozyme, cytochrome c, carbonic anhydrase, and bovine casein) in three HC. The separations were carried out at room temperature. The reasonable peak shapes and the absence of breakthrough peaks in Figure 5 (and Figure S2) confirm the presence of a homogeneous monolith that is well attached to the walls of the channel.

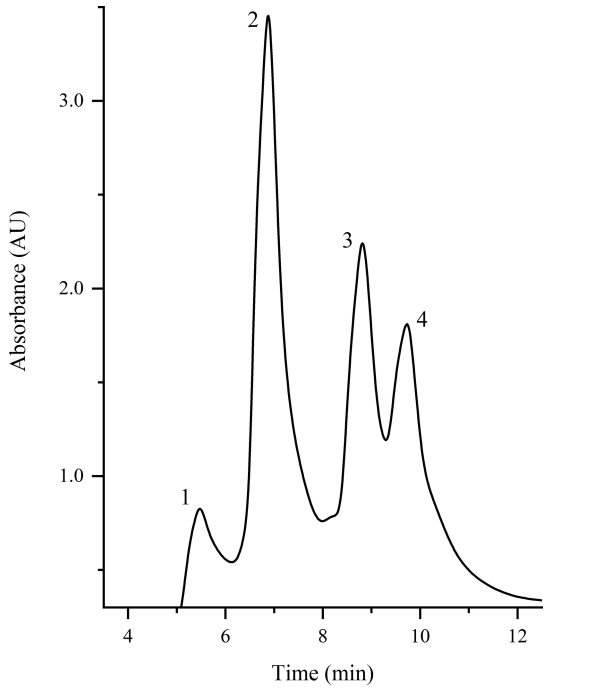

Figure 5. Separation of intact proteins on a titanium housed monolithic column within 12 min, with (1) cytochrome c, (2) lysozyme, (3) bovine casein, and (4) carbonic anhydrase. Gradient from 10% to 22% (v/v) acetonitrile in water (both solvents containing 0.1% v/v TFA) in 1 min and then on to 40% in 9 min; flow rate 35 μL/min. Separation performed at room temperature, using 1 μL loop injection and UV detection at 214 nm.

The peak widths observed in Figure 5 are high in comparison with those observed with other PS-DVB monoliths in titanium devices,[26,27] leading to a relatively low peak capacity (n_c = 12 using a 9 min gradient). Nevertheless, the repeatability of the chromatographic separations in the channels was confirmed by the low relative standard deviation of the protein retention times (see Table S2). In a device containing several parallel channels with monolithic stationary

https://dx.doi.org/10.1021/acs.analchem.9b04298
Anal. Chem. 2020, 92, 2589−2596

phases, retention times can be expected to vary by 5−7%. While such variability is not ideal, it nevertheless demonstrates the potential of these types of devices for use in spatial multidimensional liquid chromatography,[28] even with current separation performance.

The path to better thermal confinement and separations lies in pursuing higher-resolution printing methods, allowing for smaller ID channels and sharper thermal gradients. Recent metal printing methods are capable of resolutions of 15 μm, despite limitations in part sizes.[29] With suitable photopolymer substrates, stereolithographic methods can produce parts with 20 μm channels.[30,31] For monolith confinement, lower IDs can be used to better define the interface, with the main channel ID being optimized for the final chromatographic separation.

CONCLUSIONS

Poly(styrene-*co*-divinylbenzene) (PS-DVB) monoliths were successfully created by thermal polymerization in targeted regions of 3D-printed titanium devices and in inserted fused-silica capillaries. To the best of our knowledge, this is the first time that thermal polymerization was used to confine monoliths in specific regions of microfluidic devices. In comparison with UV polymerization, the thermal approach complements our choice of devices, including those with large internal diameters. The proposed approach opens the road to the utilization of a wide variety of opaque (at the desired wavelength) materials in the fabrication and application of microfluidic devices.

The thermal polymerization method can be integrated in different 3D-printed structures and in complex geometries with relative ease. With the advent of new 3D-printable materials, such as poly(ether ether ketone) (PEEK), glass, and ceramic materials, our approach represents a powerful tool to combine solvent-compatible and mechanically strong materials with diverse and customizable chemical selectivities within a single microfluidic device. However, due to different heat capacities, each material will require optimization of the polymerization conditions.

Furthermore, by using this approach of recirculating jackets for fabrication and, possibly, for device operation, sample preparation and chromatographic separation may eventually be performed within the same device. Since chromatographic separations are greatly influenced by temperature, the use of the jackets as column ovens can further enhance separations within the device. Further studies have to be performed to explore the full potential of the new approach.

ASSOCIATED CONTENT

Supporting Information

The Supporting Information is available free of charge at https://pubs.acs.org/doi/10.1021/acs.analchem.9b04298.

Figure of the 3D-printed titanium direct contact (DC) device (Figure S1a) and heating cooling/jacket (HCJ) device (Figure S1b). Inter-batch and intra-batch variation of the monolithic capillary columns thermal polymerized using the DC approach (Table S1). Chromatograms obtained from t_0 injections (Figure S2). Intra-batch variation of the retention times in different channels of the HCJ (Table S2). Infrared picture of the HCJ (Figure S3). Temperature profiles in a single channel prototype HCJ device (Figure S4a−b). 3D-printed in titanium single channel prototype HCJ device (Figure S4c). CAD of the DC and HCJ device (Figure S5a−b). (PDF)

AUTHOR INFORMATION

Corresponding Author

Marta Passamonti − *University of Amsterdam, Amsterdam, The Netherlands, and Centre for Analytical Sciences Amsterdam, Amsterdam, The Netherlands;* orcid.org/0000-0002-6691-4054; Email: m.passamonti@uva.nl

Other Authors

Ischa L. Bremer − *University of Amsterdam, Amsterdam, The Netherlands*

Suhas H. Nawada − *University of Amsterdam, Amsterdam, The Netherlands, and Centre for Analytical Sciences Amsterdam, Amsterdam, The Netherlands*

Sinéad A. Currivan − *University of Amsterdam, Amsterdam, The Netherlands, and Technological University Dublin, FOCAS Institute, Dublin, Ireland*

Andrea F. G. Gargano − *University of Amsterdam, Amsterdam, The Netherlands, and Centre for Analytical Sciences Amsterdam, Amsterdam, The Netherlands;* orcid.org/0000-0003-3361-7341

Peter J. Schoenmakers − *University of Amsterdam, Amsterdam, The Netherlands, and Centre for Analytical Sciences Amsterdam, Amsterdam, The Netherlands*

Complete contact information is available at: https://pubs.acs.org/10.1021/acs.analchem.9b04298

Notes

The authors declare no competing financial interest.

ACKNOWLEDGMENTS

The STAMP project is funded under Horizon 2020-Excellent Science-European Research Council (ERC), Project 694151. The sole responsibility of this publication lies with the authors. The European Union is not responsible for any use that may be made of the information contained therein.

REFERENCES

(1) Lämmerhofer, M.; Svec, F.; Fréchet, J. M.; Lindner, W. *J. Chromatogr. A* **2001**, *925*, 265−277.
(2) Kurganov, A. *Anal. Chim. Acta* **2013**, *775*, 25−40.
(3) Svec, F. *J. Chromatogr. B: Anal. Technol. Biomed. Life Sci.* **2006**, *841* (1−2), 52−64.
(4) Jungbauer, A.; Hahn, R. *J. Chromatogr. Libr.* **2003**, *67*, 699−724.
(5) Ehlert, S.; Rösler, T.; Tallarek, U. *J. Sep. Sci.* **2008**, *31* (10), 1719−1728.
(6) Svec, F. *Electrophoresis* **2006**, *27* (5−6), 947−961.
(7) Wouters, B.; Pirok, B. W. J.; Soulis, D.; Garmendia Perticarini, R. C.; Fokker, S.; van den Hurk, R. S.; Skolimowski, M.; Peters, R. A. H.; Schoenmakers, P. J. *Anal. Chim. Acta* **2019**, *1053*, 62.
(8) Leary, R. J.; Kinde, I.; Diehl, F.; Schmidt, K.; Clouser, C.; Duncan, C.; Antipova, A.; Lee, C.; McKernan, K.; De La Vega, F. M.; et al. *Sci. Transl. Med.* **2010**, *2* (20), 20ra14.
(9) Deverell, J. A.; Rodemann, T.; Smith, J. A.; Canty, A. J.; Guijt, R. M. *Sens. Actuators, B* **2011**, *155* (1), 388−396.
(10) Thurmann, S.; Mauritz, L.; Heck, C.; Belder, D. *J. Chromatogr. A* **2014**, *1370*, 33−39.

(11) Walsh, Z.; Abele, S.; Lawless, B.; Heger, D.; Klán, P.; Breadmore, M. C.; Paull, B.; Macka, M. *Chem. Commun.* **2008**, *7345* (48), 6504−6506.
(12) Parker, E. K.; Nielsen, A. V.; Beauchamp, M. J.; Almughamsi, H. M.; Nielsen, J. B.; Sonker, M.; Gong, H.; Nordin, G. P.; Woolley, A. T. *Anal. Bioanal. Chem.* **2019**, *411* (21), 5405−5413.
(13) Collins, D.; Nesterenko, E.; Connolly, D.; Vasquez, M.; MacKa, M.; Brabazon, D.; Paull, B. *Anal. Chem.* **2011**, *83* (11), 4307−4313.
(14) Nawada, S. H.; Aalbers, T.; Schoenmakers, P. J. *Chem. Eng. Sci.* **2019**, *207*, 1040−1048.
(15) Courtois, J.; Szumski, M.; Byström, E.; Iwasiewicz, A.; Shchukarev, A.; Irgum, K. *J. Sep. Sci.* **2006**, *29* (2), 14.
(16) Currivan, S.; Connolly, D.; Gillespie, E.; Paull, B. *J. Sep. Sci.* **2010**, *33* (4−5), 484−492.
(17) Gillespie, E.; Macka, M.; Connolly, D.; Paull, B. *Analyst* **2006**, *131* (8), 886−888.
(18) Currivan, S.; Connolly, D.; Paull, B. *Analyst* **2012**, *137* (11), 2559−2566.
(19) Collins, D. A.; Nesterenko, E. P.; Brabazon, D.; Paull, B. *Analyst* **2013**, *138* (9), 2540−2545.
(20) Connolly, D.; Barron, L. P.; Gillespie, E.; Paull, B. *Chromatographia* **2009**, *70* (5−6), 915−920.
(21) Cabot, J. M.; Duffy, E.; Currivan, S.; Ruland, A.; Jalili, R.; Mozer, A. J.; Innis, P. C.; Wallace, G. G.; Breadmore, M.; Paull, B. *Analyst* **2016**, *141* (9), 2774−2782.
(22) Darcy, H. Les Fontaines Publiques de La Ville de Dijon: exposition et application des principes à suivre et des formules à employer dans les questions de distribution d'eau.
(23) Cabooter, D.; Lynen, F.; Sandra, P.; Desmet, G. *J. Chromatogr. A* **2007**, *1157* (1−2), 131−141.
(24) Wouters, B.; De Vos, J.; Desmet, G.; Terryn, H.; Schoenmakers, P. J.; Eeltink, S. *J. Sep. Sci.* **2015**, *38* (7), 1123−1129.
(25) Yu, C.; Svec, F.; Fréchet, J. M. J. *Electrophoresis* **2000**, *21* (1), 120−127.
(26) Vonk, R. J.; Vaast, A.; Eeltink, S.; Schoenmakers, P. J. *J. Chromatogr. A* **2014**, *1359*, 162−169.
(27) Gupta, V.; Talebi, M.; Deverell, J.; Sandron, S.; Nesterenko, P. N.; Heery, B.; Thompson, F.; Beirne, S.; Wallace, G. G.; Paull, B. *Anal. Chim. Acta* **2016**, *910*, 84−94.
(28) Vanhoutte, D. J. D.; Eeltink, S.; Kok, W. T.; Schoenmakers, P. J. *Anal. Chim. Acta* **2011**, *701* (1), 92−97.
(29) Wessarges, Y.; Hagemann, R.; Gieseke, M.; Noelke, C.; Kaierle, S.; Schmidt, W.; Schmitz, K.; Haferkamp, H. *Biomed. Eng./Biomed. Technol.* **2014**, *59*, S401−S404.
(30) Gong, H.; Bickham, B. P.; Woolley, A. T.; Nordin, G. P. *Lab Chip* **2017**, *17* (17), 2899−2909.
(31) Kuo, A. P.; Bhattacharjee, N.; Lee, Y.; Castro, K.; Kim, Y. T.; Folch, A. *Adv. Mater. Technol.* **2019**, *4* (6), 1800395.

https://dx.doi.org/10.1021/acs.analchem.9b04298
Anal. Chem. 2020, 92, 2589−2596